Heliyon 9 (2023) e21414

Contents lists available at ScienceDirect

Heliyon

journal homepage: www.cell.com/heliyon

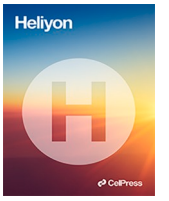

Magnetic Fe-doped TiO_2@Fe_3O_4 for metronidazole degradation in aqueous solutions: Characteristics and efficacy assessment

Farnaz Heidarinejad, Hossein Kamani *, Aramdokht Khtibi

Infectious Diseases and Tropical Medicine Research Center, Research Institute of Cellular and Molecular Sciences in Infectious Diseases, Zahedan University of Medical Sciences, Zahedan,Iran

A R T I C L E I N F O

Keywords:
Photodegradation
Magnetic nanocatalyst
UV lamp
Antibiotic
Advanced water treatment

A B S T R A C T

Antibiotics present in aquatic environments can contribute to the emergence of antibiotic-resistant bacterial strains, posing potential threats to public health. Therefore, efficient strategies to remove these compounds from water systems are essential to reduce both ecological and human health risks. This research aimed to assess the photocatalytic removal efficiency of metronidazole (MET) from an aqueous solution using a 15-W bare UVC lamp and magnetic nanocatalysts (Fe-doped TiO_2@Fe_3O_4), which were synthesized using the sol-gel technique. Furthermore, scanning electron microscopy with integrated energy dispersive X-ray analysis (SEM/EDX), X-ray diffractometry (XRD), Differential reflectance spectroscopy (DRS), vibrating sample magnetometer (VSM), and Fourier transform infrared spectroscopy (FTIR) analysis were carried out to characterize the synthesized nanocatalysts. The influence of several factors, such as pH, initial MET, and nanocatalysts concentrations during reaction times of 15–120 min, was studied. The characterization results confirmed that Fe and Ti were successfully integrated into the Fe– doped TiO_2@Fe_3O_4 nanocomposite. Highest MET degradation efficiency (99.37 %) was observed at a pH of 3, with an initial MET concentration of 60 mg/L, nanoparticle dosage of 800 mg/L, and a reaction time of 90 min. The stability of the nanocatalyst was acceptable. The results suggest that OH ions may play a crucial role in the degradation of MET demonstrating photocatalytic degradation can be an effective way to remove MET from water resources. This research sets a precedent for future endeavors aimed at harnessing photocatalysis for environmental remediation of pharmaceutical pollutants.

1. Introduction

Water pollution is an issue of global concern that poses significant threats to both the environment and human health. The contamination of water bodies by chemical, biological, and physical pollutants can have severe consequences [1–3]. Chemical pollutants are among the most common types of water pollutants and can enter water bodies through various sources such as industrial processes, agricultural practices, and household activities [4–6]. Pesticides, fertilizers, heavy metals, and industrial chemicals such as benzene and polychlorinated biphenyls are examples of chemical pollutants [7,8]. Exposure to chemical pollutants can lead to acute and chronic health effects such as respiratory problems, neurological damage, cancer, and reproductive problems [9–11]. In addition, contaminated water bodies can harm aquatic life and ecosystems, leading to decreased biodiversity and the loss of valuable ecosystem

* Corresponding author.
E-mail address: hossein_kamani@yahoo.com (H. Kamani).

https://doi.org/10.1016/j.heliyon.2023.e21414
Received 25 July 2023; Received in revised form 10 October 2023; Accepted 20 October 2023
Available online 24 October 2023

services [12]. Over the last decades, antibiotics have been widely found in the environment, posing serious human health risks. Antibiotics are often used in agriculture and aquaculture to promote growth and prevent disease in animals. However, the overuse and misuse of antibiotics can lead to the development of antibiotic-resistant bacteria, which can spread from animals to humans through contaminated water and food. This can make it difficult to treat bacterial infections in humans, leading to higher morbidity and mortality rates [13,14]. Amongst the frequently used antibiotics, MET is effective against infections originating from anaerobic bacteria and protozoa [15]. Parasites in poultry, cattle, and fish feed are also can be eliminated using MET [16]. Since MET is persistent, non-biodegradable, and highly soluble, traditional procedures are low effective in removing it from environment [17]. Due to carcinogenicity, toxicity, mutagenicity, and besides the issue of antimicrobial resistance, the accumulation of MET in aquatic environments has adverse consequences on living organisms [18]. Therefore, preserving of the ecosystem by removing MET from contaminated water supplies is crucial. Antibiotic residues may be removed from water and wastewater using a variety of processes, including adsorption and membranes, as well as biological processes [19,20]. However, there are drawbacks, such as chemical and biological sludge, adsorbent capacity limitations, adsorbent replacement and regeneration requirements, membrane filter exploitation and blockage, and the detrimental consequences of contaminants on biological systems [21,22]. Utilizing traditional and advanced oxidation techniques together is an alternative strategy for eliminating antibiotic residues and persistent contaminants from water and wastewater. Compared to traditional oxidation methods, advanced oxidation techniques are advantageous mainly due to production of highly reactive free radicals with strong oxidizing power, effectively breaking down and converting organic pollutants into harmless minerals without generating hazardous byproducts [23].

Nanoparticles are particles that are between 1 and 100 nm in size. They possess unique properties that make them highly effective in absorbing contaminants from polluted environments. Due to their small size, nanoparticles have a high surface area-to-volume ratio, which means they can interact more efficiently with the contaminants they come into contact with. Additionally, their small size allows them to penetrate through biological membranes, which makes them a useful tool for drug delivery and other applications. Magnetic nanocomposites, on the other hand, are nanoparticles that have magnetic properties [24]. These nanoparticles can be manipulated using magnetic fields, which makes them useful for many applications. In the field of contaminants remediation, magnetic nanocomposites have attracted significant attention due to their ability to efficiently remove contaminants from the environment, particularly antibiotic residues and organic pollutants [25,26]. Generally, magnetic nanoparticles has more benefits than conventional adsorbents due to its strong magnetic responses, absorption selectivity, eco-friendliness, low cost of synthesis, environmental sustainability, high build speed, regeneration, reusability, separation efficiency, and ease of use [26]. Iron nanoparticles have been the subject of numerous investigations concerning their oxidation capabilities for removing halogenated contaminants, heavy metals, and anions, including nitrates, herbicides, colorants, and antibiotic residues [27]. On the other hand, TiO_2 is widely employed in photocatalytic processes because of its non-toxicity, chemical stability, high optical activity, electron properties, and cost-effectiveness; it also has a low cost and strong photocatalytic activity and stability for antibiotic residues degradation [28]. It is the most often used semiconductor photo-catalyst for wastewater and water decontamination. In particular, several materials have been investigated, including ZnO, $ZnSnO_3$, TiO_2, $CoFe_2O_4$, Ga_2O_3, $BiVO_4$, SnO_2/Co_3O_4, $Cu_2S/Ag_2S/BiVO_4$, and Fe_3O_4/TiO_2/BC to eliminate MET [18,29–32]. However, it was shown that the presence of Fe_3O_4 plays a significant role in reducing the band gap energy and improving the photocatalytic activity of TiO_2 [33,34].

In an era where the environmental impact of pharmaceutical pollutants has become increasingly pronounced, understanding effective remediation techniques is crucial. This study delves into the synthesis of magnetic nanocatalysts Fe-doped $TiO_2@Fe_3O_4$, a potentially game-changing approach in addressing such concerns. By investigating the properties of these catalysts and evaluating their proficiency in the photocatalytic degradation of MET in aqueous solutions, we aim to establish a scientific basis that could pave the way for innovative solutions to mitigate pharmaceutical contaminants in our water systems.

2. Materials and methods

In the current experiment, the materials [deionized water, Iron (III) nitrate ($Fe(NO_3)_3$, >99 %), Nitric acid (HNO_3, 69 %), ferrous chloride ($FeCl_2 \bullet 4H_2O$, 98 %), ammonia (NH_3, 25 %), ferric chloride ($FeCl_3 \bullet 6H_2O$, >99 %), ethanol (C_2H_6O, 96 %), sulfuric acid (H_2SO_4, 98 %), titanium (IV) isopropoxide ($C_{12}H_{28}O_4Ti$, 97 %), sodium hydroxide (NaOH, >98 %)] were purchased in analytical grade from Merck Company. Moreover, the MET antibiotic (2-Methyl-5-nitroimidazole-1-ethanol) from Sigma-Aldrich (USA) was used.

2.1. Synthesis of Fe_3O_4 nanocatalysts

Adding 4.71 g of $FeCl_3 \bullet 6H_2O$ and 5 g of $FeCl_2 \bullet 4H_2O$ to 200 mL of doubly distilled water, the mixture at 600 rpm was stirred. Following this, the pH of the solution reached greater than 8 by dropwise adding 1.5 mM ammonia to it. Afterward, in the solution, a black precipitate was formed. After adding ammonia, the solution was stirred and nitrogenized for 2 h. The obtained nanocatalysts were rinsed multiple times with distilled water and then dried at room temperature after the complete reaction [35].

2.2. Synthesis of Fe-doped TiO_2@Fe_3O_4 nanocatalysts

In the present experiment, Fe-doped TiO_2@Fe_3O_4 nanocatalysts were synthesized by applying the sol-gel technique. In order to synthesize the nanocatalysts, 0.16 g, 6 drops, 4 mL and 25 mL of $Fe(NO_3)_3$, HNO_3, deionized water, and ethanol were poured intoan Erlenmeyer flask. Then, they were placed in an ultrasonic bath (60 hz) for 15 min until a uniform, the clear solution was formed (solution 1). Fe_3O_4 (0.8 gr), ethanol (400 mL), and titanium (IV) isopropoxide (A certain amount mL) were stirred to make a homogenous solution (solution 2) in a separate Erlenmeyer flask. Then, solution 1 was added to solution 2 dropwise while the two were thoroughly combined.

After both solutions were mixed for 30 min and the sol was formed, the balloon comprising sol was kept in the lab at room temperature for 5 h to form a strong adhesive gel. The produced gel was dried in an oven at 100 °C for 150 min, and then at 500 °C, the gel powder was calcined over 1 h after being washed with distilled water [36]. For structural and morphological characterizing of the synthesized Fe-doped TiO_2@Fe_3O_4 nanocatalysts, VSM, FTIR, XRD, SEM/EDX and DRS techniques were used.

2.3. Removal of MET

In this stage, the impacts of several factors on the efficacy of the photocatalytic process, including; Fe-doped TiO_2@Fe_3O_4 nanocatalyst concentration, pollutant concentration, initial pH of the solution, and UV exposure time, were evaluated. A 15-Watt UVC light was employed during the experiments. To carry out the photocatalytic procedure, the MET was prepared at different concentrations ranging from 60 to 100 mg/L and was exposed to pH levels 3, 5, 7, 9, and 11. Sodium hydroxide and sulfuric acid (0.1 N) adjusted the pH. Then, 400, 800, and 1000 mg/L of Fe-doped TiO_2@Fe_3O_4 nanocatalysts were added.

Before exposing the prepared suspensions to UVC light and initiating the photocatalytic process, the suspensions were left in the dark for 15 min to achieve adsorption-desorption equilibrium. Following this, samples of the suspensions were taken at regular intervals. The residual and starting MET concentration was determined after the separation of photocatalytic nanocatalysts. Eq. (1) represents the removal efficiency of MET based on COD [37]:

$$removal\ \% = \frac{C_i - C_o}{C_i} \times 100 \tag{1}$$

C_i initial COD and C_o residual COD in aqueous solution at 25 °C ± 2 °C in the batch system.

This study used a UV-C tube lamp, model G15T8 (Philips, Holland), as the irradiation source to investigate its effects on a sample under controlled conditions. The UV-C tube lamp had a power rating of 15 W and dimensions of 451 mm in length and 2.5 cm in diameter. The lamp emitted radiation at a wavelength of 253.4 nm. In the experimental setup, the UV lamp was strategically positioned within a specially chamber, de-signed to rigorously limit the ingress of extraneous light. A predetermined and constant distance of 10 cm was maintained between the light source and the reactor, a parameter meticulously considered to optimize photo-catalytic performance. Within this controlled environment, both temperature and relative humidity were assiduously regulated at 25 °C and 50 % respectively, ensuring consistent conditions and mitigating potential experimental deviations.

The lamp was installed in a light-infiltrated chamber to minimize interference from external light sources. The chamber had a controlled environment with temperature, and humidity maintained at 25 °C and 50 %, respectively.

3. Results and discussion

3.1. SEM analysis

The SEM is a powerful tool used for analyzing the morphology of materials. In this particular study, SEM was utilized to estimate the shape and size distribution of nanocatalysts, specifically Fe_3O_4 and Fe-doped TiO_2@Fe_3O_4 catalysts. The results obtained from SEM images showed that there was no noticeable variation in the surface morphology of the nanocatalysts after the synthesis of doped nanoparticles. However, the particles tended to aggregate, which could be attributed to their magnetic characteristics and fineness [38]. Fig. 1a shows that the Fe_3O_4 are formed separately and have a size of 20–32 nm (Average = 26.3 nm). They have almost smooth surfaces in some places and tend to agglomerate. As Fig. 1a shows, after covering the nanocatalysts Fe_3O_4 with Fe-doped TiO_2, the pores between the nanocatalysts Fe_3O_4 are almost closed, which indicates the presence of the surface coating Fe_3O_4 (the average size of 61.7 nm).

The EDX spectra for Fe_3O_4 and Fe-doped TiO_2@Fe_3O_4 nanoparticles are shown in Fig. 1b. The spectra for Fe_3O_4 show peaks corresponding to Fe and O, with weight percentages of 72.6 % and 27.3 %, respectively. The spectra for Fe-doped TiO_2@Fe_3O_4 show peaks corresponding to Ti, Fe, and O, with weight percentages of 62.4 %, 14.9 %, and 22.7 %, respectively. The EDX analysis confirms the presence of Fe in both Fe_3O_4 and Fe-doped TiO_2@Fe_3O_4 nanoparticles. The weight percentage of Fe in Fe-doped TiO_2@Fe_3O_4 is lower than that in Fe_3O_4, indicating that some of the Fe in Fe-doped TiO_2@Fe_3O_4 is incorporated into the TiO2 matrix. The EDX analysis also confirms the presence of Ti and O in Fe-doped TiO_2@Fe_3O_4, indicating the successful synthesis of Fe-doped TiO_2@Fe_3O_4 nanoparticles.

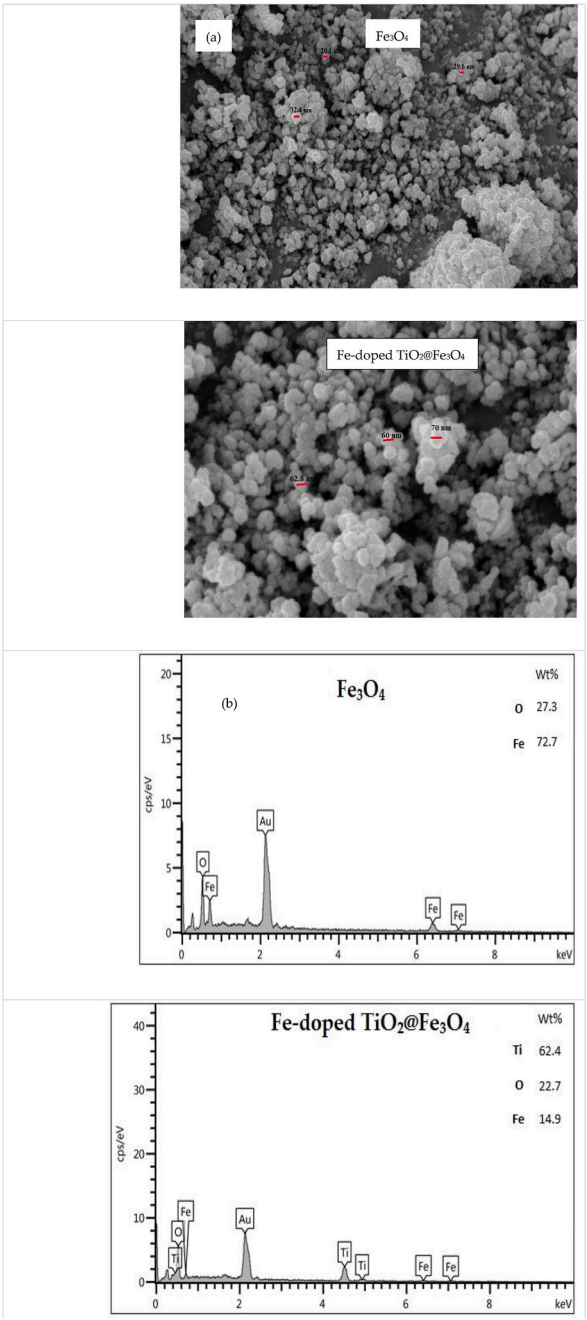

Fig. 1. SEM/EDX images of Fe_3O_4 and Fe-doped TiO_2@Fe_3O_4 nanocatalysts.

3.2. XRD analysis

The Fe_3O_4 nanocatalysts (Fig. 2a) displayed an X-ray diffraction (XRD) pattern consisting of seven distinct peaks (18.23°, 30.16°, 35.12°, 43.14°, 53.50°, 57.05°, 62.51°), indicative the typical cubic inverse spinel structure of Fe_3O_4 [39,40]. The synthesized Fe-doped TiO_2@Fe_3O_4 (Fig. 2b) displayed well-defined peaks in its XRD spectrum, suggesting a superior crystalline structure. The Fe-doped TiO_2@Fe_3O_4 diffraction pattern exhibited several distinct peaks (24.06°, 25.32°, 27.47°, 33.28°, 35.78°, 40.93°, 47.98°, 49.80°, 54.20°, 57.65,° 62.11°, 64.09°, and 69.21°). Peaks at 25.32°, 47.98°, 54.20°, and 69.21° were attributed to the TiO_2 anatase phase, while peaks at 27.47°, 35.78°, and 40.93° were assigned to the planes of rutile, indicating the presence of both phases in TiO_2. Peaks at 35.78°, 54.20°, 57.65°, and 62.11° were consistent with diffraction from the Fe3O4. The patterns above have been employed in accordance with the JCPDS Card numbers 89–3854, 21–1272, 019–0629, 21–127, and 79–0418 [33,39,41,42]. The research

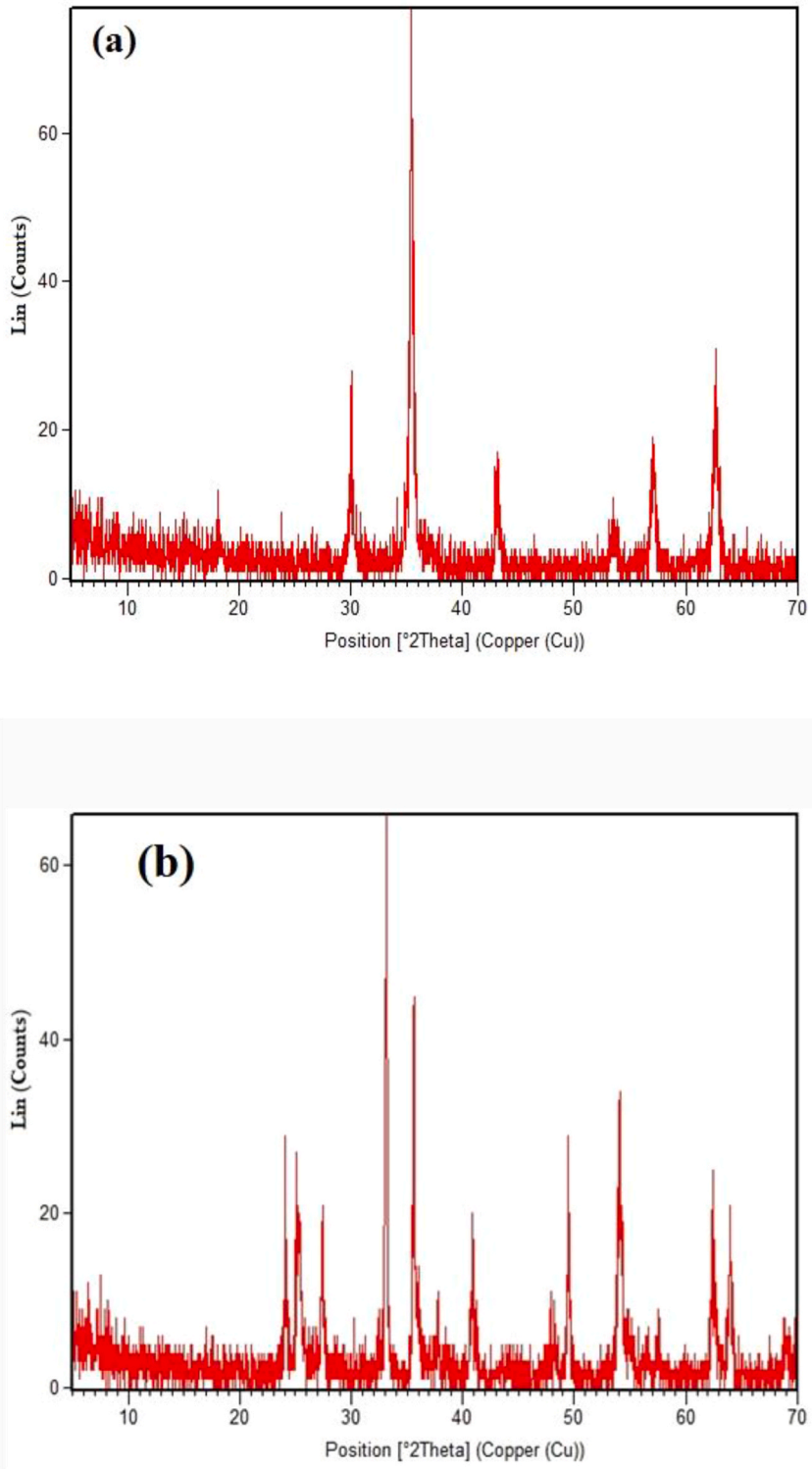

Fig. 2. XRD of (a) Fe_3O_4 nanocatalysts (b) Fe-doped TiO_2@Fe_3O_4 nanocatalysts.

conducted by Sheikhmohammadi and colleagues involved the characterization of TiO_2@Fe_3O_4 nanocatalyst. The analysis of the nanocatalyst revealed the presence of three crystal phases, namely anatase phase, rutile phase, and cubic phase [33]. Furthermore, the findings of the present investigation exhibit concurrence with the outcomes of Shojaei's previous research concerning the utilization of Fe^{3+}/TiO_2@Fe_3O_4 nanocatalyst [42].

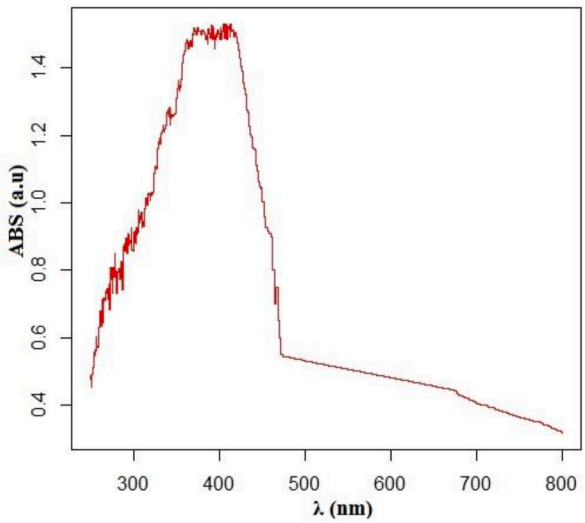

Fig. 3. DRS of Fe– doped TiO_2@Fe_3O_4 composite.

3.3. DRS analysis

Differential Reflectance Spectroscopy is a vital tool for accurately discerning the optical characteristics of materials. It's instrumental in determining the band gap energy of materials, a parameter central to understanding their electronic and optical behaviors. In this study, DRS analysis of the Fe– doped TiO_2@Fe_3O_4 nanocatalyst revealed a band gap of 2.7 eV. This is distinctively lower than the 3.2 eV band gap intrinsic to unaltered TiO_2, as shown in Fig. 3. This deviation is ascribed to the introduction of iron oxide into the composite. In essence, the integration of Fe_3O_4 with TiO_2 results in a heterojunction, which alters the electronic structure of TiO_2 and consequently narrows its band gap. This observation resonates with prior research, such as the study by Nada et al. on. on $ZnFe_2O_4$@TiO_2 nanofibers [43].

The Fe–doped TiO_2@Fe_3O_4 nanocatalyst, by virtue of its composition comprising TiO_2, Fe–TiO_2, and Fe_3O_4 nanoparticles and its reduced band gap of 2.7 eV, displays heightened photocatalytic activity. The heterojunction between TiO_2 and Fe_3O_4 enhances charge transfer, effectively improving the separation of photogenerated electron-hole pairs. The positioning of the valence band (VB) and conduction band (CB) in both TiO_2 and Fe_3O_4 are determinants in this electron and hole migration, thereby elevating the overall charge separation efficiency.

3.4. VSM analysis

To effectively isolate and recycle nanocatalysts, those with magnetic properties are favored. To assess the magnetic traits of the produced nanocatalysts, VSM analysis was utilized, and the results are illustrated in Fig. 4, showing the highest saturation

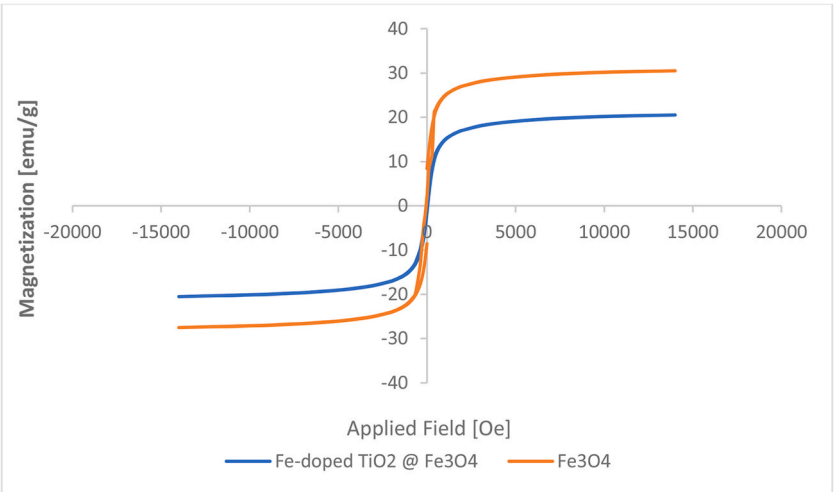

Fig. 4. VSM of synthesized nanocatalysts Fe_3O_4 sample and sample Fe-doped TiO_2 @ Fe_3O_4 nanocatalysts.

magnetization values for Fe_3O_4 and Fe–doped TiO_2@Fe_3O_4 nanocatalysts. The findings demonstrate that every sample has super-paramagnetic characteristics. In our study, the highest value of magnetic properties in Fe_3O_4 was obtained higher than that of magnetic properties for Fe-doped TiO_2@Fe_3O_4. The saturation magnetization of uncoated and coated samples decreased after applying a TiO_2 coating. This decline in magnetization can be attributed to the presence of a non-magnetic titania shell around the Fe_3O_4 core, which reduces the overall mass of the core. This reduction in magnetization serves as evidence for the successful deposition of titania on the magnetite nanoparticle. It supports the idea that the coated titania is bonded to the surface of the magnetite particles through Fe–*O*–Ti chemical bonding. Previous research has also reported a reduction in the magnetic moment of iron ions bound to Ti on the surface of magnetite particles through Fe–*O*–Ti bonding. For example, Abbas and colleagues found that the saturation magnetite of the uncoated magnetite sample with titanium was 80 emu/g. In comparison, the sample coated with titanium exhibited a decrease in saturation magnetization of about 57 emu/g, similar to our study [44].

3.5. FTIR analysis

FTIR can display a scan of the infrared spectrum absorbed by the sample. The material is identified based on the frequency of the infrared spectrum that is absorbed by the sample and the strength of this absorption. Fig. 5 shows only the peaks related to functional groups in nanocomposite Fe–doped TiO_2@Fe_3O_4 nanocatalysts. Ti–*O*–Ti vibrational mode and pure TiO_2 belonging to the bending vibrations of the C–H bond were located in the range 478.76–685.87 cm^{-1} and 1395.74 cm^{-1}. Also, the weak absorption band at around 2354.55 and 2309.60 cm^{-1} belonged to the Fe-doped TiO_2 spectrum [45]. The band was observed in the 2926.96 cm^{-1} related to CH_2 stretching bond [46]. The spectral regions between 3429.45 and 1614.65 cm^{-1} indicate the stretching vibration of O–H groups and the bending vibration of adsorbed water molecules, respectively. This information is based on research by Saroj [47]. The study

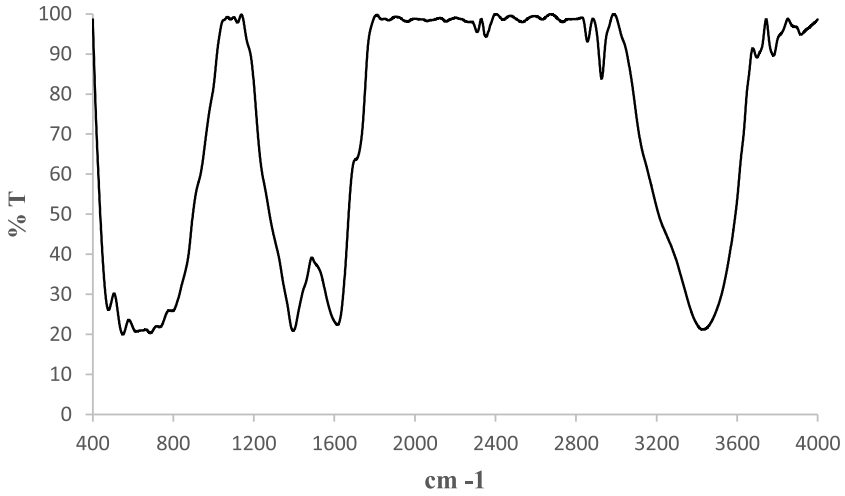

Fig. 5. FTIR of Fe–doped TiO_2@Fe_3O_4 nanocatalysts.

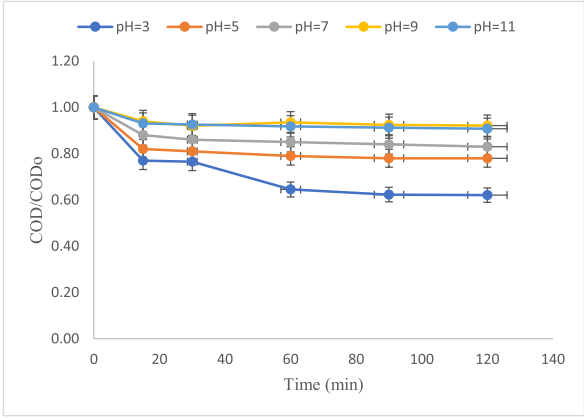

Fig. 6. Influence of initial pH values in degradation of MET (initial MET concentration of 60 mg/L, nanocatalyst dosage of 400 mg/L, and reaction time of 90 min) evaluated at different times.

conducted by Craciun and colleagues suggests that the slight variation in peak positions for the doped sample could be explained by substituting Fe^{3+} in the titanium dioxide structure or by the presence of non-crystalline iron oxides at the periphery of the titanium dioxide crystals [48].

3.6. Effect of initial pH on the removal of MET

The pH of a solution plays a pivotal role in modulating the degradation kinetics of pollutants during photocatalytic processes, particularly under UV-C irradiation. As depicted in Fig. 6, the efficiency of MET degradation using Fe–doped TiO_2@Fe_3O_4 nanocatalysts was evaluated under varying pH conditions—acidic, neutral, and basic—over different time intervals, keeping other parameters constant. It was observed that MET degradation was notably enhanced in acidic environments, with optimal degradation recorded at pH 3. In contrast, the degradation efficiency attenuated under neutral and basic conditions, reaching an equilibrium after approximately 90 min. This equilibrium signifies a dynamic state where the rate of MET degradation matches the rate of MET regeneration, resulting in no apparent net change in its concentration. The observed pH influence can be attributed to the protonation of MET, which possesses an imidazole functional group, facilitating its adsorption onto the catalyst's surface [49] Kamani et al. emphasized that pH variations markedly affect the generation of hydroxyl radicals, potent oxidizing entities, during advanced oxidation processes [50]. This corroborates with the findings of Asgari et al. and Abdoli et al., both of whom delineated that a more acidic milieu augments MET removal efficiency. The underpinning mechanism can be associated with the enhanced production and availability of hydroxyl radicals in acidic conditions, which accelerate the photocatalytic degradation of MET [51,52].

3.7. Effect of initial concentration on the removal of MET

Having identified the optimal pH, the influence of various concentrations of MET, including 60, 80, and 100 mg/L, on the removal efficiency was examined (Fig. 7). In this case, the highest MET removal efficiency was observed at the lower initial concentrations of MET. The MET removal efficiency declined, in contrast to rising pollutant concentrations. As depicted in Fig. 7, highest efficiency was achieved at a MET concentration of 60 mg/L, and it declined with increasing MET concentration up to 100 mg/L. The most important factor controlling the photocatalytic degradation rate is the production and transfer of active groups [53]. When the pollutant concentration decreases, higher oxidation rates are common, which is due to the limited amount of reactive species that are responsible for their degradation. Farzadkia and colleagues reported outcomes that were similar [54].

3.8. Effect of nanocatalyst dosage on the removal of MET

The dosage of nanocatalysts or catalysts used in hybrid and catalytic oxidation processes is one of the most significant factors influencing the processes' optimal performance. The impact of Fe-doped TiO_2@Fe_3O was investigated using a variety of dosages (400, 800, and 1000 mg/L). As seen in Fig. 8, increasing the concentration of nanocatalysts up to 800 mg/L enhanced the degradation efficiency. However, increasing the concentration to 1000 mg/L lowered the degradation. Adding more Fe-doped TiO_2@Fe_3O_4 nanocatalysts can result in more MET molecules being adsorbed on the surface, simultaneously elevating the amount of •OH radicals in the solution. For this reason, more MNZ molecules are exposed to photodegradation. However, the high nanocatalyst dosage (1000 mg/L) leads to the deactivation of the activated molecules by collision with ground-state molecules, which regulate and dominate the reaction. Thus, the reaction rate stayed unchanged and might be reduced again [55]. These results were consistent with Sheikhmohammadi's study on the removal of MET by TiO_2/Fe_3O_4 nanocatalyst [33].

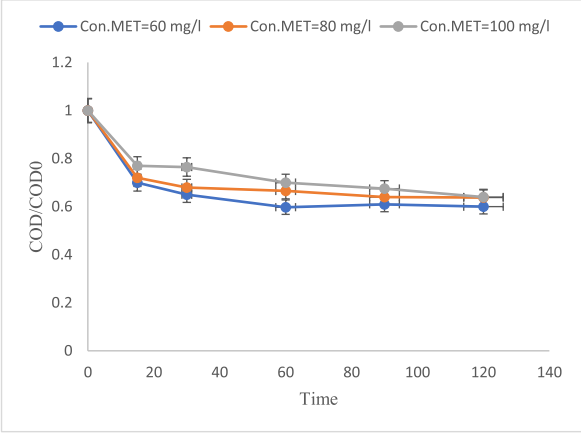

Fig. 7. Effect of initial concentration in degradation of MET (pH = 3, nanocatalyst dosage of 400 mg/L, and reaction time of 90 min), evaluated at different times.

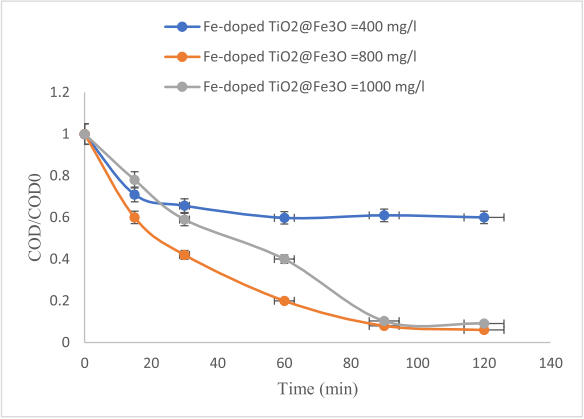

Fig. 8. Effect of Fe-doped TiO_2@Fe_3O dosage on photocatalytic degradation of MET (pH = 3, initial MET concentration of 60 mg/L, and reaction time of 90 min), evaluated at different times.

3.9. Possible mechanism of degradation for MET

The elucidation of degradation mechanisms is critical in comprehending the functioning of a material and its deg-radation over time in a given environment [53,56]. It is imperative to optimize and improve the efficiency of a material by identifying the factors responsible for its degradation. Identifying such factors is important in determining the material's durability and devising strategies to enhance its stability and resistance to degradation [57–59]. This aspect has thus garnered significant attention from researchers in the scientific community. MET can be degraded using magnetic Fe-doped TiO2@Fe3O4 through photocatalytic degradation. The reaction can be represented as follows:

When Fe-doped TiO2@Fe3O4 is irradiated with UV-C light, electrons in the VB absorb energy and are excited to the CB, creating electron-hole pairs:

$$\text{Fe-doped TiO2@Fe3O4} + h\nu \rightarrow \text{Fe-doped TiO2@Fe3O4 (e-/h+)} \quad (2)$$

$$\text{MET} + \text{Fe-doped TiO2@Fe3O4} \rightarrow \text{MET/ Fe-doped TiO2@Fe3O4} \quad (3)$$

Upon absorption of a photon, the MET molecule in the adsorbed state is excited to form a MET radical action (MET*):

$$\text{MET} + h\nu \rightarrow \text{MET}^* + \text{e-} \quad (4)$$

The MET* reacts with the hydroxyl radicals (•OH) generated on the surface of Fe-doped TiO2@Fe3O4 to form a degraded product of MET:

$$\text{MET}^* + \bullet\text{OH} \rightarrow \text{degraded product of MET} \quad (5)$$

The degraded product of MET can further undergo degradation reactions to form smaller and less harmful compounds. Factors such as pH, initial MET concentration, nanocatalyst concentration, and reaction time influence the degradation efficiency of MET using magnetic Fe-doped TiO2@Fe3O4. The optimal conditions for highest MET degradation efficiency (99.37%) were observed at a pH of 3, with an initial MET concentration of 60 mg/L, nanoparticle dosage of 800 mg/L, and a reaction time of 90 min.

3.10. The stability of the photocatalyst

This study aimed to assess the stability of a newly synthesized photocatalyst. After optimizing the oxidation conditions, the nanocatalyst was subjected to multiple cycles of MET photodegradation. Subsequently, the photocatalyst was isolated (centrifugation), purified (ethanol and water), and dried at 60 °C for 2 h to prepare it for analysis. The effectiveness of the photocatalyst was determined by quantifying the remaining amount after each round of photocatalysis. The findings indicate that the nanocatalyst is highly stable, as demonstrated by the preservation of 99.3 %, 97.9 %, 96.8 %, and 94.4 % of its initial activity following four consecutive rounds of MET photocatalysis.

3.11. Study limitations

This investigation on the photocatalytic efficiency of Fe-doped TiO_2@Fe_3O_4 nanocatalysts, synthesized via a sol-gel method, yielded promising results under controlled laboratory conditions. However, real-world scenarios might present deviations in environmental factors like MET concentrations and other co-existing contaminants. Furthermore, while MET degradation was achieved under identified optimal conditions, the nature and environmental implications of the derivative by-products remain inadequately

addressed. The recovery, reusability, and long-term stability of the nanocatalysts also necessitate further exploration. To solidify the method's eco-compatibility claim, broader environmental impact studies, encompassing energy metrics and residual nanoparticles' fate, are imperative.

4. Conclusions

The present study successfully synthesized Fe-doped TiO_2@Fe_3O_4 nanocatalysts using a simple sol-gel method and demonstrated their efficiency in the photocatalytic oxidation of MET from aqueous solutions. Fe ions were successfully integrated into the TiO_2 nanocatalyst, as confirmed by characterization results. The study found that the photocatalytic efficiency depended on the pH, initial MET concentration, nanocatalyst dosage, and reaction time. The highest MET degradation efficiency was observed at pH 3, initial MET concentration of 60 mg/L, nanocatalyst dosage of 800 mg/L, and reaction time of 90 min under the irradiation of a 15-W UVC lamp. The findings of this study highlight the potential of using photocatalytic oxidation with Fe-doped TiO_2@Fe_3O_4 nanocatalysts to treat MET-containing wastewater. The insights gleaned suggest that this modality could be pivotal in refining water treatment protocols aimed at MET removal, with its cardinal merits being its operational simplicity, pronounced efficacy, and eco-compatibility. Nonetheless, the forward path mandates comprehensive investigations to finetune this photocatalytic modality for authentic wastewater scenarios and to decipher potential environmental ramifications, particularly concerning derivative by-product genesis.

Funding

This work was supported by the thank Zahedan University of Medical Sciences (Grant number: 9797).

Data availability Statement

Data will be made available on request.

CRediT authorship contribution statement

Farnaz Heidarinejad: Conceptualization, Data curation, Investigation, Methodology, Software, Writing – original draft. **Hossein Kamani:** Conceptualization, Formal analysis, Investigation, Project administration, Supervision, Validation, Writing – review & editing. **Aramdokht Khtibi:** Conceptualization, Methodology, Validation, Writing – review & editing.

Declaration of generative AI and AI-assisted technologies in the writing process

We leveraged artificial intelligence to enhance the quality of the manuscript.

Declaration of competing interest

The authors declare that they have no known competing financial interests or personal relationships that could have appeared to influence the work reported in this paper.

Acknowledgments

This research is a part of the approved thesis of Zahedan University of Medical Sciences (Grant number: 9797, Ethics code IR.ZAUMS.REC.1399.331). The authors thank Zahedan University of Medical Sciences for funding this research.

References

[1] E. Norabadi, S.D. Ashrafi, H. Kamani, A. Jahantiq, Degradation of 2,6-dichlorophenol by Fe-doped TiO2Sonophotocatalytic process: kinetic study, intermediate product, degradation pathway, Int. J. Environ. Anal. Chem. 2020 (2020) 1–16, https://doi.org/10.1080/03067319.2020.1837122.
[2] Y. Jari, N. Roche, M.C. Necibi, S. El Hajjaji, D. Dhiba, A. Chehbouni, Emerging pollutants in Moroccan wastewater: occurrence, impact, and removal technologies, J. Chem. 2022 (2022), https://doi.org/10.1155/2022/9727857.
[3] H. Kamani, S.D. Ashrafi, A. Jahantiq, E. Norabadi, M. Dashti Zadeh, Catalytic degradation of humic acid using Fe–doped TiO2 - ultrasound hybrid system from aqueous solution, Int. J. Environ. Anal. Chem. (2021), https://doi.org/10.1080/03067319.2021.1979535.
[4] H. Ouachtak, A. El Guerdaoui, R. El Haouti, R. Haounati, H. Ighnih, Y. Toubi, F. Alakhras, R. Rehman, N. Hafid, A.A. Addi, M.L. Taha, Combined molecular dynamics simulations and experimental studies of the removal of cationic dyes on the eco-friendly adsorbent of activated carbon decorated montmorillonite Mt@AC, RSC Adv. 13 (2023) 5027–5044, https://doi.org/10.1039/d2ra08059a.
[5] A. Jahantiq, R. Ghanbari, A.H. Panahi, S.D. Ashrafi, A.D. Khatibi, E. Noorabadi, A. Meshkinian, H. Kamani, Photocatalytic degradation of 2,4,6-trichlorophenol in aqueous solutions using synthesized fe-doped tio 2 nanoparticles via response surface methodology, Desalin. Water Treat. 183 (2020) 366–373, https://doi.org/10.5004/dwt.2020.25249.
[6] H. Kamani, G.H. Safari, G. Asgari, S.D. Ashrafi, Data on modeling of enzymatic elimination of direct red 81 using response surface methodology, Data Br 18 (2018) 80–86, https://doi.org/10.1016/j.dib.2018.03.012.
[7] H. Societies, H. Rehman, M. Munir, K. Ashraf, K. Fatima, S. Shahab, B. Ali, Analysis of Drinking Water Quality in the Newly Developed, 2022, pp. 1–16.
[8] L. Montano, C. Pironti, G. Pinto, M. Ricciardi, A. Buono, C. Brogna, M. Venier, M. Piscopo, A. Amoresano, O. Motta, Polychlorinated biphenyls (PCBs) in the environment: occupational and exposure events, effects on human health and fertility, Toxics 10 (2022), https://doi.org/10.3390/toxics10070365.

[9] R. Proshad, T. Kormoker, M.S. Islam, M.A. Haque, M.M. Rahman, M.M.R. Mithu, Toxic effects of plastic on human health and environment : a consequences of health risk assessment in Bangladesh, Int. J. Heal. 6 (2017) 1, https://doi.org/10.14419/ijh.v6i1.8655.

[10] A. Hossein Panahi, A. Meshkinian, S.D. Ashrafi, M. Khan, A. Naghizadeh, G. Abi, H. Kamani, Survey of sono-activated persulfate process for treatment of real dairy wastewater, Int. J. Environ. Sci. Technol. 17 (2020) 93–98, https://doi.org/10.1007/s13762-019-02324-4.

[11] E. Norabadi, A.H. Panahi, R. Ghanbari, A. Meshkinian, H. Kamani, S.D. Ashrafi, Optimizing the parameters of amoxicillin removal in a photocatalysis/ozonation process using Box–Behnken response surface methodology, Desalin. Water Treat. 192 (2020) 234–240, https://doi.org/10.5004/dwt.2020.25728.

[12] I. Bashir, F.A. Lone, R.A. Bhat, S.A. Mir, Z.A. Dar, S.A. Dar, Concerns and threats of contamination on aquatic ecosystems, in: Bioremediation Biotechnol. Sustain. Approaches to Pollut. Degrad., Springer International Publishing, 2020, pp. 1–26, https://doi.org/10.1007/978-3-030-35691-0_1.

[13] J.H. Ramírez-Franco, L.A. Galeano, M.A. Vicente, Fly ash as photo-Fenton catalyst for the degradation of amoxicillin, J. Environ. Chem. Eng. 7 (2019), https://doi.org/10.1016/j.jece.2019.103274.

[14] M. Tian, X. He, Y. Feng, W. Wang, H. Chen, M. Gong, D. Liu, J.L. Clarke, A. Van Eerde, Pollution by antibiotics and antimicrobial resistance in live stock and poultry manure in China, and countermeasures, Antibiotics 10 (2021), https://doi.org/10.3390/antibiotics10050539.

[15] X. Wu, W.J. Shen, A. Deshpande, A.O. Olaitan, K.L. Palmer, K.W. Garey, J.G. Hurdle, The integrity of heme is essential for reproducible detection of metronidazole-resistant clostridioides difficile by agar dilution susceptibility tests, J. Clin. Microbiol. 59 (2021), e0058521, https://doi.org/10.1128/JCM.00585-21.

[16] R. Vishwakarma, V. Dhaka, T.U. Ariyadasa, A. Malik, Exploring algal technologies for a circular bio-based economy in rural sector, J. Clean. Prod. 354 (2022), https://doi.org/10.1016/j.jclepro.2022.131653.

[17] A. Seidmohammadi, Y. Vaziri, A. Dargahi, H.Z. Nasab, Improved degradation of metronidazole in a heterogeneous photo-Fenton oxidation system with PAC/Fe3O4 magnetic catalyst: biodegradability, catalyst specifications, process optimization, and degradation pathway, Biomass Convers. Biorefinery. 13 (2023) 9057–9073, https://doi.org/10.1007/s13399-021-01668-7.

[18] N. Davari, M. Farhadian, A.R. Solaimany Nazar, Synthesis and characterization of Fe2O3 doped ZnO supported on clinoptilolite for photocatalytic degradation of metronidazole, Environ. Technol. 42 (2021) 1734–1746, https://doi.org/10.1080/09593330.2019.1680738.

[19] Z.Y. Lu, Y.L. Ma, J.T. Zhang, N.S. Fan, B.C. Huang, R.C. Jin, A critical review of antibiotic removal strategies: performance and mechanisms, J. Water Process Eng. 38 (2020), 101681, https://doi.org/10.1016/j.jwpe.2020.101681.

[20] M.N. Alnajrani, O.A. Alsager, Removal of antibiotics from water by polymer of intrinsic microporosity: isotherms, kinetics, thermodynamics, and adsorption mechanism, Sci. Rep. 10 (2020) 1–14, https://doi.org/10.1038/s41598-020-57616-4.

[21] N. Nasrollahi, V. Vatanpour, A. Khataee, Removal of antibiotics from wastewaters by membrane technology: limitations, successes, and future improvements, Sci. Total Environ. 838 (2022), 156010, https://doi.org/10.1016/j.scitotenv.2022.156010.

[22] P.R. Yaashikaa, P.S. Kumar, A. Saravanan, D.V.N. Vo, Advances in biosorbents for removal of environmental pollutants: a review on pretreatment, removal mechanism and future outlook, J. Hazard Mater. 420 (2021), https://doi.org/10.1016/j.jhazmat.2021.126596.

[23] R. Kishor, D. Purchase, G.D. Saratale, R.G. Saratale, L.F.R. Ferreira, M. Bilal, R. Chandra, R.N. Bharagava, Ecotoxicological and health concerns of persistent coloring pollutants of textile industry wastewater and treatment approaches for environmental safety, J. Environ. Chem. Eng. 9 (2021), https://doi.org/10.1016/j.jece.2020.105012.

[24] P. Bhatt, S. Gangola, G. Bhandari, W. Zhang, D. Maithani, S. Mishra, S. Chen, New insights into the degradation of synthetic pollutants in contaminated environments, Chemosphere 268 (2021), https://doi.org/10.1016/j.chemosphere.2020.128827.

[25] M. Dubey, R. Kumar, S.K. Srivastava, M. Joshi, Visible light induced photodegradation of chlorinated organic pollutants using highly efficient magnetic Fe3O4/TiO2 nanocomposite, Optik 243 (2021), https://doi.org/10.1016/j.ijleo.2021.167309.

[26] N. Nasseh, B. Barikbin, L. Taghavi, M.A. Nasseri, Adsorption of metronidazole antibiotic using a new magnetic nanocomposite from simulated wastewater (isotherm, kinetic and thermodynamic studies), Compos. Part B Eng. 159 (2019) 146–156, https://doi.org/10.1016/j.compositesb.2018.09.034.

[27] M.I. Litter, A short review on the preparation and use of iron nanomaterials for the treatment of pollutants in water and soil, Emergent Mater 5 (2022) 391–400, https://doi.org/10.1007/s42247-022-00355-1.

[28] N.H. Mohamad Idris, K.Y. Cheong, B.J. Kennedy, T. Ohno, H.L. Lee, Buoyant titanium dioxide (TiO2) as high performance photocatalyst and peroxide activator: a critical review on fabrication, mechanism and application, J. Environ. Chem. Eng. 10 (2022), https://doi.org/10.1016/j.jece.2022.107549.

[29] L. Cai-Yun, Y. Zheng-Feng, B. Paul, Facile synthesis of spinel CoFe 2 O 4 nanoparticle and its application as magnetic recoverable photocatalyst for degradation of metronidazole and some selected organic dyes, J. Nanosci. Nanotechnol. 20 (2019) 1209–1214, https://doi.org/10.1166/jnn.2020.16963.

[30] S. Fakhravar, M. Farhadian, S. Tangestaninejad, Excellent performance of a novel dual Z-scheme Cu2S/Ag2S/BiVO4 heterostructure in metronidazole degradation in batch and continuous systems: immobilization of catalytic particles on α-Al2O3 fiber, Appl. Surf. Sci. 505 (2020), https://doi.org/10.1016/j.apsusc.2019.144599.

[31] S. Dong, L. Cui, W. Zhang, L. Xia, S. Zhou, C.K. Russell, M. Fan, J. Feng, J. Sun, Double-shelled ZnSnO3 hollow cubes for efficient photocatalytic degradation of antibiotic wastewater, Chem. Eng. J. 384 (2020), https://doi.org/10.1016/j.cej.2019.123279.

[32] F. Asgharzadeh, M. Gholami, A.J. Jafari, M. Kermani, H. Asgharnia, R.R. Kalantary, Heterogeneous photocatalytic degradation of metronidazole from aqueous solutions using Fe3O4/TiO2 supported on biochar, Desalin. Water Treat. 175 (2020) 304–315, https://doi.org/10.5004/dwt.2020.24789.

[33] A. Sheikhmohammadi, E. Asgari, H. Nourmoradi, M.M. Fazli, M. Yeganeh, Ultrasound-assisted decomposition of metronidazole by synthesized TiO2/Fe3O4 nanocatalyst: influencing factors and mechanisms, J. Environ. Chem. Eng. 9 (2021), 105844, https://doi.org/10.1016/j.jece.2021.105844.

[34] T. Barkhade, I. Banerjee, Photocatalytic degradation of Rhodamine B dye using Fe doped TiO2 nanocomposites, in: AIP Conf. Proc., American Institute of Physics Inc., 2018, 030016, https://doi.org/10.1063/1.5035218.

[35] Z. Es'haghi, A. Nezhadali, A.D. Khatibi, Magnetically responsive polycaprolactone nanoparticles for progesterone screening in biological and environmental samples using gas chromatography, Anal. Bioanal. Chem. 408 (2016) 5537–5549, https://doi.org/10.1007/s00216-016-9650-5.

[36] H. Kamani, S. Nasseri, M. Khoobi, R. Nabizadeh Nodehi, A.H. Mahvi, Sonocatalytic degradation of humic acid by N-doped TiO2 nano-particle in aqueous solution, J. Environ. Heal. Sci. Eng. 14 (2016) 1–9, https://doi.org/10.1186/s40201-016-0242-2.

[37] G. El-Sayed, H. Jahin, S. Ibrahim, G.O. El-Sayed, H.A. Dessouki, H.S. Jahin, S.S. Ibrahiem, Photocatalytic degradation of metronidazole in aqueous solutions by copper oxide nanoparticles nanotechnology view project water quality view project photocatalytic degradation of metronidazole in aqueous solutions by copper oxide nanoparticles, J. Basic Environ. Sci. 1 (2014) 102–110. https://www.researchgate.net/publication/280494248.

[38] R. Wang, X. Wang, X. Xi, R. Hu, G. Jiang, Preparation and photocatalytic activity of magnetic Fe3O 4/SiO2/TiO2 composites, Adv. Mater. Sci. Eng. 2012 (2012), https://doi.org/10.1155/2012/409379.

[39] G.S. Shahane, K. Zipare, J. Dhumal, S. Bandgar, V. Mathe, G. Shahane, Superparamagnetic manganese ferrite nanoparticles: synthesis and magnetic properties size-controlled synthesis and characterization of superparamagnetic Mn-Zn ferrite nanoparticles for ferrofluid application view project synthesis of ferrite nanoparticles for ferrofluid application view project superparamagnetic manganese ferrite nanoparticles: synthesis and magnetic properties, J. Nanosci. Nanoeng. 1 (2015) 178–182.

[40] S. Khashan, S. Dagher, N. Tit, A. Alazzam, I. Obaidat, Novel method for synthesis of Fe3O4@TiO2 core/shell nanoparticles, Surf. Coatings Technol. 322 (2017) 92–98, https://doi.org/10.1016/j.surfcoat.2017.05.045.

[41] G. Pucar Milidrag, J. Nikić, V. Gvoić, A. Kulić Mandić, J. Agbaba, M. Bečelić-Tomin, D. Kerkez, Photocatalytic degradation of magenta effluent using magnetite doped TiO2 in solar parabolic trough concentrator, Catalysts 12 (2022) 1–20, https://doi.org/10.3390/catal12090986.

[42] A.F. Shojaei, A. Shams-Nateri, M. Ghomashpasand, Magnetically recyclable Fe3+/TiO2@Fe3O4 nanocomposites towards degradation of direct blue 71 under visible-light irradiation, Micro & Nano Lett. 12 (2017) 161–165, https://doi.org/10.1049/mnl.2016.0620.

[43] A.A. Nada, M. Nasr, R. Viter, P. Miele, S. Roualdes, M. Bechelany, Mesoporous ZnFe2O4@TiO2 nanofibers prepared by electrospinning coupled to PECVD as highly performing photocatalytic materials, J. Phys. Chem. C 121 (2017), https://doi.org/10.1021/acs.jpcc.7b08567.

[44] M. Abbas, B. Parvatheeswara Rao, V. Reddy, C. Kim, Fe3O4/TiO2 core/shell nanocubes: single-batch surfactantless synthesis, characterization and efficient catalysts for methylene blue degradation, Ceram. Int. 40 (2014) 11177–11186, https://doi.org/10.1016/j.ceramint.2014.03.148.

[45] A. El Mragui, Y. Logvina, O. Zegaoui, J.C.G. Esteves, Photocatalytic activity under visible irradiation toward carbamazepine degradation, Green Chem. 18 (2019) 4–6.
[46] N. Rani, B.S. Dehiya, Magnetic core-shell Fe3O4@TiO2 nanocomposites for broad spectrum antibacterial applications, IET Nanobiotechnol. 15 (2021) 301–308, https://doi.org/10.1049/nbt2.12017.
[47] S. Saroj, L. Singh, R. Ranjan, S.V. Singh, Enhancement of photocatalytic activity and regeneration of Fe-doped TiO 2 (Ti 1−x Fe x O 2) nanocrystalline particles synthesized using inexpensive TiO 2 precursor, Res. Chem. Intermed. 45 (2019) 1883–1906, https://doi.org/10.1007/s11164-018-3708-2.
[48] E. Craciun, L. Predoana, I. Atkinson, I.J.-… of P. and, U, Fe3+-doped TiO2 Nanopowders for Photocatalytic Mineralization of Oxalic Acid under Solar Light Irradiation, Elsevier, 2018 (n.d. https://www.sciencedirect.com/science/article/pii/S1010603017304963. (Accessed 16 February 2023).
[49] A. Kumar, A review on the factors affecting the photocatalytic degradation of hazardous materials, Mater. Sci. Eng. Int. J. 1 (2017) 106–114, https://doi.org/10.15406/mseij.2017.01.00018.
[50] H. Kamani, E. Bazrafshan, S.D. Ashrafi, F. Sancholi, Efficiency of sono-nano-catalytic process of Tio2 nano-particle in removal of erythromycin and metronidazole from aqueous solution, J. Maz. Univ. Med. Sci. 27 (2017) 140–154. https://jmums.mazums.ac.ir/article-1-9523-en.html. (Accessed 16 February 2023).
[51] A. Abdoli, R. Shokuhi, A.M.S. Mohammadi, G. Asgari, Survey of catalytic O zonation process with MgO modified activated carbon for the removal of metronidazole from aqueous solutions through a fluidized bed reactor, J. Sabzevar Univ. Med. Sci. 23 (2016) 84–94.
[52] E. Asgari, A. Sheikhmohammadi, J. Yeganeh, Application of the Fe3O4-chitosan nano-adsorbent for the adsorption of metronidazole from wastewater: optimization, kinetic, thermodynamic and equilibrium studies, Int. J. Biol. Macromol. 164 (2020) 694–706, https://doi.org/10.1016/j.ijbiomac.2020.07.188.
[53] B. Wang, Z. Li, H.X. Ma, J.B. Zhang, L.Y. Jiao, H. Hao, E.Z. Liu, L. Xu, C. Wang, B. Zhou, X.X. Ma, Dynamic construction of self-assembled supramolecular H12SubPcB-OPhCOOH/Ag3PO4 S-scheme arrays for visible photocatalytic oxidation of antibiotics, Appl. Catal. B Environ. 318 (2022), 121882, https://doi.org/10.1016/j.apcatb.2022.121882.
[54] M. Farzadkia, E. Bazrafshan, A. Esrafili, J.K. Yang, M. Shirzad-Siboni, Photocatalytic degradation of Metronidazole with illuminated TiO2 nanoparticles, J. Environ. Heal. Sci. Eng. 13 (2015) 1–8, https://doi.org/10.1186/s40201-015-0194-y.
[55] M. Esmati, A. Allahresani, A. Naghizadeh, Synthesis and characterization of Graphitic Carbon Nitride/Mesoporous Nano-Silica (g-C3N4/KCC-1) nanocomposite as a novel highly efficient and recyclable photocatalyst for degradation of antibiotic in aqueous solution, Res. Chem. Intermed. 47 (2021) 1447–1469, https://doi.org/10.1007/s11164-020-04358-7.
[56] X. Li, K. Yang, C. Yu, S. Yang, K. Zhang, W. Dai, H. Ji, L. Zhu, W. Huang, S. Ouyang, Advances towards the utilization of Vis-NIR light energy by coating YF3:Yb3+,Er3+ over ZnS microspheres triggering hydrogen production and pollutants disposal, J. Mater. Chem. C 7 (2019) 8053–8062, https://doi.org/10.1039/c9tc02068c.
[57] K. Zhang, J. Guan, P. Mu, K. Yang, Y. Xie, X. Li, L.Z.-D, undefined, Visible and Near-Infrared Driven Yb 3+/Tm 3+ Co-doped InVO 4 Nanosheets for Highly Efficient Photocatalytic Applications, Rsc.Org, Pubs, 2020 (n.d.), https://pubs.rsc.org/en/content/articlehtml/2020/dt/d0dt02318c. (Accessed 8 March 2023).
[58] K. Shi, F. Wang, X. Li, W. Huang, K.Q. Lu, C. Yu, K. Yang, MIL-53(Fe)@perylene diimide all-organic heterojunctions for the enhanced photocatalytic removal of pollutants and selective oxidation of benzyl alcohol, Catalysts 13 (2023), https://doi.org/10.3390/catal13030471.
[59] R. Haounati, F. Alakhras, H. Ouachtak, T.A. Saleh, G. Al-Mazaideh, E. Alhajri, A. Jada, N. Hafid, A.A. Addi, Synthesized of zeolite@Ag2O nanocomposite as superb stability photocatalysis toward hazardous rhodamine B dye from water, Arab. J. Sci. Eng. 48 (2023) 169–179, https://doi.org/10.1007/s13369-022-06899-y.